Reactive orbital energy theory serving a theoretical foundation for the electronic theory of organic chemistry

Tsuneda, Takao
Sumitomo, Hiroki
Hasebe, Masatoshi
Tsutsumi, Takuro
Taketsugu, Tetsuya

(Citation)
Journal of Computational Chemistry,44(2):93-104

(Issue Date)
2023-01-15

(Resource Type)
journal article

(Version)
Accepted Manuscript

(URL)
https://hdl.handle.net/20.500.14094/0100477600

Reactive orbital energy theory serving a theoretical foundation for the electronic theory of organic chemistry

Takao Tsuneda*

Department of Chemistry, Faculty of Science,
Hokkaido University, Sapporo 060-0810, Japan and
Graduate School of Science Technology and Innovation,
Kobe University, Nada-ku, Kobe, Hyogo 657-8501, Japan

Hiroki Sumitomo

Department of Chemistry, Faculty of Science,
Hokkaido University, Sapporo 060-0810, Japan

Masatoshi Hasebe

Graduate School of Chemical Sciences and Engineering,
Hokkaido University, Sapporo 060-0810, Japan

Takuro Tsutsumi

Department of Chemistry, Faculty of Science,
Hokkaido University, Sapporo 060-0810, Japan and
L-Station, Creative Research Institution (CRI),
Hokkaido University, Sapporo 060-0812, Japan

Tetsuya Taketsugu

Department of Chemistry, Faculty of Science,
Hokkaido University, Sapporo 060-0810, Japan and
Institute for Chemical Reaction Design and Discovery (WPI-ICReDD),
Hokkaido University, Sapporo 001-0021, Japan

Abstract

It is established that the reactive orbital energy theory (ROET) theoretically reproduces the rule-based electronic theory diagrams of organic chemistry by a comparative study on the charge transfer natures of typical organic carbon-carbon and carbon-heteroatom bond formation reactions: aldol, Mannich, α-aminooxylation and isogyric reactions. The ROET, which is an expansion of the reaction electronic theories (e.g., the frontier orbital theory) in terms of orbital energies, elucidates the reactive orbitals driving reactions and the charge transferability indices of the reactions. Performing the ROET analyses of these reactions shows that the charge transfer directions given in the rule-based diagrams of the electronic theory are reproduced even for the functional groups of charge transfer destinations in all but only two processes for 38 reaction processes. The ROET analyses also make clear the detailed orbital-based pictures of these bond formation reactions: i.e., the use of the out-of-plane antibonding π orbitals in acidic conditions (enol-mode) and in-plane antibonding π orbitals in basic conditions (enolate-mode), which explain the experimentally-assumed mechanisms such as the π-bond formations in acidic conditions and σ-bond formations at α-carbons in basic conditions. Furthermore, the ROET analyses explicate that the methyl group initially accepts electrons and then donates them to the bond formations in the target reactions. It is, consequently, suggested that the ROET serves a theoretical foundation for the electronic theory of organic chemistry.

*Electronic address: tsuneda@phoenix.kobe-u.ac.jp

I. INTRODUCTION

Reaction electronic theories have been developed to analyze reactions by electronic movements on the basis of the bonding natures, charge transferability and molecular orbital (MO) shapes. In conventional reaction electronic theories, there are the electronic theory of organic chemistry [1, 2], the frontier orbital theory [3] and the conceptual density functional theory (DFT) [4–6]. The electronic theory of organic chemistry is a rule-based reaction electronic theory using the connections of stable reasonance structures, which are drawn based on the electronegativities, octet rule, bond natures and electrophilicities, in order to presume the electronic movements for revealing the reactivities and the directions of reactions [7]. So far, this theory has been established through the feedback from experimental results and plays the central role in organic syntheses and interpretations of reactions. The frontier orbital theory basically targets at the directions of reactions based on the electronic distributions and orbital phases of frontier orbitals, i.e., highest occupied MO (HOMO), lowest unoccupied MO (LUMO) and their closely-lying orbitals [3]. The conceptual DFT forms the foundation for the frontier orbital theory [8] and has produced various chemical indices, which are used as tools for analyzing chemistry [6], based on the concept of DFT. Though these conventional reaction electronic theories provide intuitive interpretation to reactions, they have limitations in their applicability to a wide variety of reactions.

Reactive orbital energy theory (ROET) [9, 10] is the reaction electronic theory that investigates reactions using orbital energy variations in the structural deformations of reactions based on the theorem analogous to Fukui function f of conceptual DFT [11],

$$f = \left(\frac{\partial \mu}{\partial v}\right)_N = \left(\frac{\partial \epsilon_{\text{outermost}}}{\partial v}\right)_N, \tag{1}$$

where μ, v, N and $\epsilon_{\text{outermost}}$ are chemical potential, external electron-nuclei potential, the number of electrons and outermost orbital energy, respectively. According to Eq. (1), reaction analysis based on this theory, which is called "ROET analysis", requires quantitative occupied and unoccupied orbital energies accurately satisfying the generalized Koopmans theorem [12], which are currently obtained only by long-range corrected (LC) DFT [13]. In this analysis, the occupied and unoccupied valence orbitals giving the most varied orbital energies through the reaction processes are defined as reaction-driving orbitals called "reactive orbitals" [9]. This analysis also determines whether the reactions are charge transfer (CT)-driven or structural deformation (dynamics)-driven on the basis of the gradient of

the orbital energy gaps between the occupied and unoccupied reactive orbitals through the reaction paths [9, 14]. Based on the ROET analysis, it is recently found that there is the one-to-one correspondence between reaction pathways and reactive orbitals, implying the possibility of the unification of potential energy-based theories and the electronic theories [15]. Applying the ROET analysis to reaction analyses can quantitatively reveal electronic movements for various types of reactions that have never been targeted in conventional reaction electronic theories.

Since carbon-carbon and carbon-heteroatom bond formation reactions are typical reactions in experimental organic syntheses, these reactions have been major subjects in the electronic theory of organic chemistry. Aldol and Mannich reactions are organic carbon-carbon (C-C) bond formation reactions proceeding in both acidic and basic conditions through the generation of carbocations and carbanions, respectively, which are representative intermediates using electron distribution gradients for accelerating bond formations in many organic reactions [7]. In acidic conditions, these reactions proceed in the enol-mode: carbocations are initially generated from ketones or aldehydes accepting protons, and then they are transformed into the enols promoting the C-C bond formations through the π conjugations. These reactions, on the other hand, use the enolate-mode in basic conditions: carbanions are produced at first from ketones or aldehydes accepting electrons, and then they are transformed into the enolatese forming the C-C bonds at the α carbons. α-Aminooxylation [16] and isogyric [17] reactions form the carbon-heteroatom bonds in basic conditions. For all these reactions, it is theoretically established that long-range exchange interactions play a significant role probably due to their charge transfer natures [18]. Aldol and Mannich reactions are canonical reactions of organic syntheses, which have been targeted even in the textbooks of the electronic theory of organic chemistry [7] for explaining the electron movements driving their acidic and basic reactions. Moreover, α-aminooxylation and isogyric reactions are carbon bond formation reactions that will be useful for discussing the bond formation reactions from other viewpoints. Note that these reactions are involved in the synthetic reactions of organocatalysis in enantioselective chemistry [17]. We, therefore, consider that the reactions are appropriate as subjects for examining the relation between the ROET analysis and the electronic theory of organic chemistry.

In this study, the ROET analysis reveals the relation between their electron movements of the ROET analyses with the electronic theory diagrams of organic chemistry, which have,

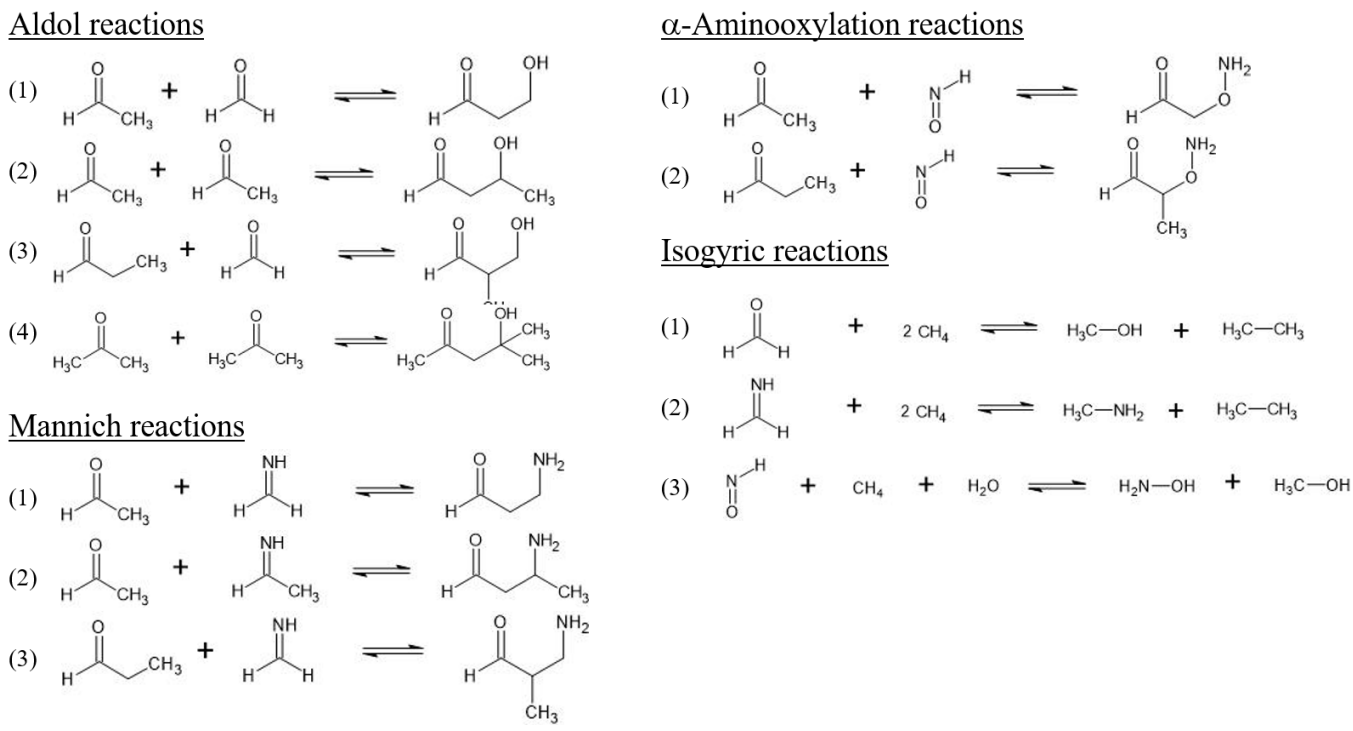

FIG. 1: Calculated reactions: four aldol, three Mannich, two α-aminooxylation and three isogyric reactions.

so far, no clear theoretical background but are corrected by the feedback of experiments, by applying to the carbon bond formation reactions, aldol, Mannich, α-aminooxylation and isogyric reactions,

II. COMPUTATIONAL DETAILS

Kohn-Sham DFT [19, 20] calculations are performed for the forward and backward processes of four aldol, three Mannich, two α-aminooxylation and three isogyric reactions (Fig. 1), with a LC+vdW method [21, 22] combining LC-DFT [23–25] with the local response dispersion (LRD) correlation functional [26]. For aldol, Mannich, and α-aminooxylation reactions, the enol- and enolate-mode reactions, which correspond to the reaction mechanisms in acid and basic conditions, respectively, are examined (Fig. 2). The LC-DFT uses the long-range correction for the Becke 1988 (B88) exchange [27] + one-parameter progressive (OP) correlation [28] functional (LC-BOP) with the aug-cc-pVTZ basis set [29]. In the LC-DFT calculations, the parameter $\mu_{\rm LC}$ is set as 0.33, though it is set as 0.47 only for aldol (4)

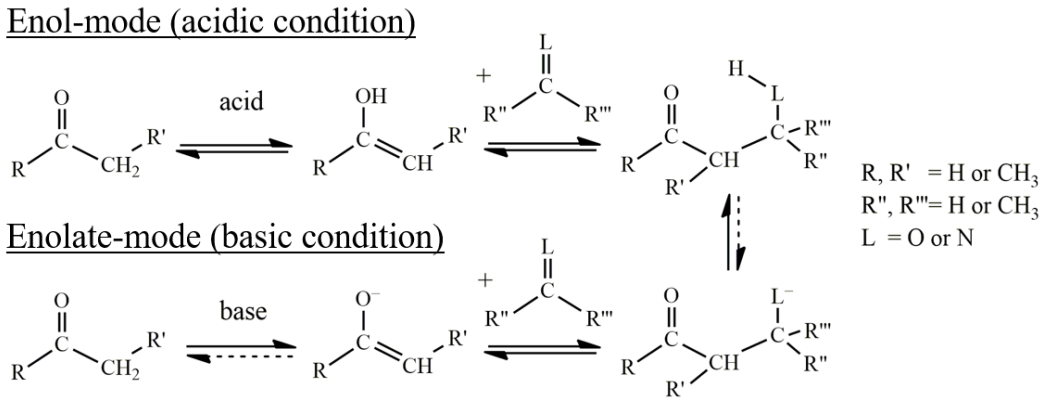

FIG. 2: Enol- and enolate-mode mechanisms of calculated ketones for aldol and Mannich reactions.

reaction in the enol-mode and α-aminooxylation (1) reaction in the enolate-mode in order to determine their transition state (TS) geometries. The TS geometries are determined using the single-component artificial force induced reaction (SC-AFIR) method [30] in GRRM17 program [31, 32]. Based on the determined TS geometries, the intrinsic reaction coordinate (IRC) calculations are performed using the Gonzalez-Schlegel method (version 2) [33] (for the calculated IRCs, see Fig. S1 of the supporting information). All calculations are carried out with GAMESS-US program [34].

The ROET analyses are performed using the calculated IRCs of the reaction paths and the molecular orbital energies at the geometries on the IRCs as follows [10, 15]:

1. Plotting the valence orbital energies for each IRC, the orbital energies are, first, traced along the IRCs for three reaction processes: reactant complex to product complex, reactant molecules to reactant complex, and product complex to product molecules. In our original orbital energy-tracing program, the molecular orbital giving the maximum overlap between the succeeding points is automatically picked out, while if the picked orbital would be multiplicated, the orbital giving the minimum orbital energy gradients for the orbital energies at the anteroposterior steps is selected.

2. The occupied and unoccupied valence orbitals giving the most stabilized (decreased) and most destabilized (increased) orbital energies are then chosen for the orbital energies traced along the IRC of the reaction process between the reactant and product complexes as the occupied and unoccupied reactive orbitals. In this study, the va-

lence orbitals are assumed as the set of 10 highest occupied and 10 lowest unoccupied orbitals for avoiding arbitrariness.

3. Using the occupied and unoccupied reactive orbitals on the IRC, the normalized reaction diagram is illustrated by plotting the normalized orbital energy gap along the normalized IRC,

$$\bar{\Delta}_{\mathrm{gap}} = \frac{\Delta_{\mathrm{gap}} - \Delta_{\mathrm{gap}}^{\mathrm{initial}}}{\Delta_{\mathrm{gap}}^{\mathrm{terminal}} - \Delta_{\mathrm{gap}}^{\mathrm{initial}}}, \tag{2}$$

where $\Delta_{\mathrm{gap}}^{\mathrm{initial}}$ and $\Delta_{\mathrm{gap}}^{\mathrm{terminal}}$ are the orbital energy gaps at the initial and terminal steps of each IRC.

4. The reactive orbital energy gap gradient is evaluated at the initial reaction step (i.e., the structure of not the reactant molecules but the reactant complex) on the normalized IRC, $\bar{v}$, for each forward or backward process, and then, the inverse of the reactive orbital energy gap divided by four, $\left|\nabla_{\bar{v}}\bar{\Delta}_{\mathrm{gap}}\right|^{-1}/4$, which is called "charge transferability index", is calculated. The IRC of charge transferability index higher than or equal to one is evaluated as CT-driven, while other IRCs being dynamics-driven.

5. Finally, the reactive orbital diagram is drawn using the images of the reactive orbitals with the charge transferability indices at the geometries of the reactant molecules, reactant complex, TSs, product complex, and product molecules for each process. The diagram is called "ROET diagram". In this ROET diagram, the charge transfer between the occupied and unoccupied reactive orbitals at the reactant molecules is interpreted to drive the initial reaction process, while the charge transfer of the occupied reactive orbitals along the overall reaction process is explained to drive the whole reaction process.

Note that if the chosen occupied and unoccupied reactive orbitals are assigned to the same reactant molecule in step 2, the most destabilized orbital belonging to another molecule is alternatively selected for the consistency of reaction. As a result, the second most destabilized orbitals are picked out for the enol-mode of aldol reaction (2) and Mannich reaction (2). We have found no other orbital pairs, which are needed to represent the reactions in the present ROET analyses. Based on the above-mentioned one-to-one correspondence between the reactive orbital pairs and reaction pathways [15], we consider that the main

occupied and unoccupied orbital pair drives each reaction pathway and that the orbitals of equivalent orbital energy variations are subject to the main orbital pair. We should also think of subsequent barrierless reaction processes that might connect to the main processes. Since these subsequent processes cause wrong reaction-driving charge transfers, they should be excluded from the ROET analysis. For more details of the reactive orbital energy theory analyses, see our previous articles [10, 15].

III. RESULTS AND DISCUSSION

A. ROET analyses of aldol reactions in the enol- and enolate-modes

Let us first explore four types of aldol reactions in the enol-mode: i.e., the C-C bond formations of enol (ethenol or 1-propenol or 2-propenol) with aldehyde (formaldehyde or acetaldehyde) molecules. The IRCs of these reactions are summarized with the reactant, product and TS geometries in Fig. S1-1 of the supporting information. Figure 3 shows the reactive orbitals and charge transferability indices for the aldol reactions in the enol-mode with the comparison to their diagrams based on the electronic theory of organic chemistry, which is henceforth called "the electronic theory diagrams". The figure shows the variations of the occupied and unoccupied reactive orbitals in the forward and backward processes for the reaction equations of the aldol reactions in the enol-mode in Fig. 1. For the reactant and product molecules, the molecules, in which the occupied and unoccupied reactive orbitals belong, are attached. The charge transferability indices of the reactive orbital energy theory are also given as the numbers in between the reactive orbitals of the reactant complexes and those of the transition state (TS) structures, while these are also shown as solid and dotted curve arrows of electron transfers attaching the reactive orbitals of the reactant complexes for the CT- and dynamics-driven processes, respectively. At the leftmost of the forward processes and the rightmost of the backward processes, the electronic theory diagrams are illustrated. Note that the electronic theory diagrams obeying the rule of the electronic theory [7] are uniquely determined for these and all other reactions calculated in this study except for the positions of charges in the presence of equivalent functional groups mentioned later.

As shown in the figure, the forward bond formation processes give the identical reactive

orbitals for the same enol reactant molecules. The occupied reactive orbitals are determined as unique out-of-plane antibonding (nonbonding C-O bonding C-C) π orbitals centering on the carbonyl carbons of enols, which are in the shape of bonding orbitals for the C-OH bonds and C=C bonds, while the unoccupied reactive orbitals are given as various antibonding π orbitals. According to the electronic theory diagrams, the electron of the O-H bond of an enol initially activates the C=C double bond to form a new C-C bond with an aldehyde. The ROET analysis supports all these diagrams and suggests how these reactions electronically proceed: the out-of-plane antibonding π orbitals of the enols induce and conjugate with the antibonding π orbitals of the aldehydes to form the C-C bonds. Since the antibonding π orbitals have the nodes at the carbonyl carbons, the C-C bonds are formed at the α-carbon of the enols. The variations of the occupied reactive orbitals also indicate that all the charge transfers in the whole reactions are consistent with those of the electronic theory diagrams. As shown in the figure, the small charge transferability indices except for reaction (2), however, determine that these reactions are dynamics-driven. This suggests that these forward bond formation processes are initially driven by structural deformations, which may be attributed to the proton transfers. Note that charge transferability indices increase by adding the methyl group in the electron-donating molecules. This supports the dynamics-driven natures of these reactions, because this indicates that the steric effects are larger than the electron-donating effects for the methyl groups in these reactions.

For the backward bond dissociation processes, the charge transfers in the whole reactions are consistent with those of the electronic theory diagrams, because all the unoccupied reactive orbitals correspond to the destinations of the charge transfers in the diagrams: i.e., the carbonyl C=O double bonds. The reactive orbitals show electrons transfer from the occupied orbitals with nodes at the α-carbons to the unoccupied antibonding π orbitals centering on the C-OH bonds. Consequently, the charge transfers cause the polarizations of electron distributions leading to the C-C bond dissociations. Note, however, that the backward processes are also determined as dynamics-driven due to the small charge transferability indices similar to the forward processes. It is, therefore, expected that the proton transfers drive the backward processes.

Next, let us explore the aldol reactions in the enolate-mode, i.e., the C-C bonds are formed between enolate (ethenolate or 1-propenolate or 2-propenolate) anions with aldehyde (formaldehyde or acetaldehyde or acetone) molecules. The IRCs of the enolate-mode

reactions are compiled in Fig. S1-2 of the supporting information with the reactant, product and TS geometries. The reactive orbitals and charge transferability indices for the aldol reactions in the enolate-mode are compared to their diagrams of the electronic theory diagrams in Fig. 4.

For the forward bond formation processes, the reactive orbitals of the reactant molecules in Fig. 4 show that the directions of charge transfers between molecules are consistent with the electronic theory diagrams except for reaction (2). The occupied reactive orbitals are in-plane antibonding π orbitals centering on the carbonyl carbons, which are conjugated with the C=O, C-H and C-C bondings, for all these processes. According to the variation of the occupied reactive orbitals, the C-C bond formations proceed through the conjugation of the antibonding π orbitals with the C-C σ bonds. That is, the C-C bonds are formed by overlapping the leafstalk parts of the in-plane antibonding π orbitals in the form of four-leaf clover. Another significant finding is the opposite charge transfer direction against that of the electronic theory diagram for reaction (2), indicating that this reaction is driven not by the charge difference but by the charge transfer between the reactive orbitals corresponding to the bonding orbital form of the product. Actually, the population analysis of the reactant complex naturally leads to the conclusion that electrons transfer from the enolate anion in the charge of -0.995 (Mulliken) or -0.807 (Löwdin). The in-plane antibonding π orbital is also present as HOMO-1 as shown in the occupied reactive orbital of reaction (1). Nevertheless, the charge transfer driving this reaction proceeds from acetaldehyde to the enolate anion. This indicates that the methyl group provides high electron-donating ability resisting the charge bias to the in-plane antibonding π orbital forming C-C bonds. For this result, the most convincing interpretation is that the methyl group initially accepts electrons when forming the reactant complex, and then donates them to form the C-C bond.

Figure 4 also shows that the charge transfers initially proceed to the same directions of the electronic theory diagrams except for reaction (2) but go on to the opposite directions as a whole. For reaction (2), opposite charge transfer directions are given for the electronic theory diagram and ROET diagram due to the difference in the carbonyl groups with negative charges. This discrepancy comes from the conventional concept of the methyl group that the methyl group is simply electron-donating. As mentioned for the forward processes, the methyl group initially accepts electrons. This result supports this new concept for the methyl group. As seen in the analyses of the enol-mode reactions, the bond dissociations

lead to the localization of the electron distributions. The reactive orbitals indicate that electrons initially transfer from the in-plane π bond of the C-O^- group to the lone pair orbital of the oxygen atom of the C=O double bond, and subsequently move in the opposite direction to localize in formaldehyde and dimethyl ketone through the structural deformations. The large charge transferability indices indicate that all these reactions are CT-driven in the initial processes. Interestingly, it is also experimentally found that in basic conditions, aldol reactions uniquely need a kinetic control of very low temperature ($-78°$C)[7], despite reactions (2) and (4) are calculated to be endothermic in the forward processes between the reactant and product complexes (see Fig. S1-2 in the supporting information). This experimental finding implies that the charge transfer directions due to the structural deformations in the backward processes need to be controlled to smoothly perform the bond formations in the aldol reactions.

B. ROET analyses of Mannich reactions in the enol- and enolate-modes

Similar to aldol reactions, Mannich reactions also proceed through the enol-mode in acidic conditions. This study targets three types of Mannich reactions: i.e., the C-C bond formations of enol (ethenol or 1-propenol) with imine (methanimine or ethanimine) molecules. In Fig. S1-3 of the supporting information, the IRCs of these reactions are compiled with the reactant, product and TS geometries. The reactive orbitals and charge transferability indices in Fig. 5 are arranged for the Mannich reactions in the enol-mode comparing to the electronic theory diagrams.

According to the small charge transferability indices in Fig. 5, all the forward processes are determined as dynamics-driven, implying that proton transfers initially activate these reactions. The reactive orbitals in the figure indicate that electrons initially transfer from the enols to the imines in consistent with those of the electronic theory diagrams. Different from the above-mentioned aldol reactions, the occupied reactive orbitals are determined as the out-of-phase bonding π orbitals across the C=C and C-OH bonds for reactions (1) and (2), while the antibonding π orbital is similarly specified as the occupied reactive orbital for reaction (3). This determination is attributed to the bonding orbitals of the products. For the unoccupied reactive orbitals, the in-phase antibonding π orbitals of the C=N double bonds of the imines are induced through the structural deformations. These results indicate

that the bond formations of the Mannich reactions in the enol-mode proceed through the π-conjugations, as has been experimentally proposed for enol-mode reactions [7].

For all the backward processes of the enol-mode Mannich reactions, Fig. 5 indicates that the antibonding π orbitals, which have nodes at the dissociated bonds, are the occupied reactive orbitals, while the antibonding π orbitals of the carbonyl groups are the unoccupied reactive orbitals. The charge transfer directions derived from the reactive orbitals are consistent with those of the electronic theory diagrams. Similar to the bond dissociations of the aldol reactions, the electrons transfer between the reactive orbitals localize the electron distributions. The small charge transferability indices determine that these reaction processes are dynamics-driven. Based on these results, it is interpreted that proton transfers induce the charge transfers to the carbonyl groups to form the localized electron distributions causing the bond dissociations. This interpretation is consistent with the electronic theory diagrams of these processes.

Next, let us explore the corresponding Mannich reactions in the enolate-mode in basic conditions: i.e., the C-C bond formations of enolate (ethenolate or 1-propenolate) anions with imine (methanimine or ethanimine) molecules. The IRCs of these reactions are shown with the reactant, product and TS geometries in Fig. S1-4 of the supporting information. In Fig. 6, the reactive orbitals and charge transferability indices of the Mannich reactions in the enolate-mode are compared to these electronic theory diagrams.

For the enolate-mode, the large charge transferability indices and reactive orbitals in Fig. 6 show that the forward processes are CT-driven through the charge transfers from the in-plane antibonding π orbitals of the enols to the lone pair orbitals of the N atoms of the imines. This result is consistent with the electronic theory diagrams for the charge transfer directions (from the enols to the imines) and for the destinations of the electron transitions (the N orbitals of the C=NH groups). Note that the occupied reactive orbitals, i.e., the in-plane antibonding π orbitals of the enols, are the same as those of the enolate-mode aldol reactions (1), (3) and (4), indicating that this four-leaf-type π orbital plays a main role in enolate-mode reactions. The figure also shows that the presence of the methyl groups significantly affect the quantity of charge transfers: i.e., the charge transfers are large for the electron-donating enol containing the methyl group, while being small for the electron-accepting imine containing the methyl group. The reactive orbitals of the reactant molecules indicate that this comes from the electronic property of the methyl group that

initially accept and then donate electrons in bond formations, as seen for the aldol reactions.

The figure also shows that in the backward processes of the enolate-mode, the occupied reactive orbitals are the lone pair orbitals of the N atoms of the C=NH^- group, while the unoccupied ones are the π orbitals of the O atoms of the carbonyl groups. As is illustrated from these reactive orbitals, the initial charge transfers are consistent with the corresponding electronic theory diagrams. The reactive indices determine that reactions (1) and (2) are dynamics-driven, while reaction (3) is CT-driven. Note that this depends on the presence of the methyl group after the bond dissociations. That is, the reaction is CT-driven if the methyl group is in the enol-side, while being dynamics-driven if the methyl group is in the imine-side. Note also that the electron localizations to one side of the molecules in bond dissociations proceed in the opposite directions of the initial reaction processes in the whole enolate-mode processes: i.e., the electrons are localized in the imines. This implies that in bond dissociations, antibonding orbitals are stabilized to weaken the bonds and then the electrons are localized in one side of dissociated molecules.

C. ROET analyses of α-aminooxylation reactions

α-Aminooxylation reactions proceed to form C-O bonds in the enolate-mode in basic conditions. This study targets the C-O bond formations of enolate (ethenolate or 1-propenolate) anions with nitrosyl hydride molecule. In the supporting information, Fig. S1-5 illustrates the IRCs of these reactions with the reactant, product and TS geometries. Note that these two reactions are contrasting: reaction (1) is endothermic even from the separated reactant molecules, while reaction (2) being exothermic even from the reactant complex. The reactive orbitals and charge transferability indices of the α-aminooxylation reactions in the enolate-mode are shown in Fig. 7.

For the forward processes, Fig. 7 indicates that these reactions give different unoccupied reactive orbitals despite of the same electron-accepting molecule, while providing similar occupied reactive orbitals, i.e., the antibonding π orbitals of the enolates, similar to those of the above-mentioned enolate-mode reactions. The reactive orbitals indicate that the charge transfer directions are both consistent with these electronic theory diagrams: i.e., from the C=C double bonds of the enolates to the O=N double bonds of the nitrosyl hydride. Nevertheless, the charge transferability indices also determine different results: reaction

(1) is dynamics-driven, while reaction (2) being CT-driven. These results may come from the above-mentioned difference in the reaction energies and reaction barriers. Since the difference between these reactions is only the presence of the methyl group in the enolate molecules, these results suggest that the methyl group enhances the charge transferability index and the stability of products in reactions by initially accepting electrons and then donating them to form bonds.

The reactive orbitals of the backward processes in Fig. 7 show that the occupied ones are both the bonding π orbitals across the reactant molecules, while the unoccupied ones depending on the reactions: i.e., the lone pair orbital of the NH group for reaction (1) and the antibonding π orbital of the C=O double bond for reaction (2). Note that the direction of charge transfer is opposite to that of the electronic theory diagram for reaction (1). In contrast, the variation of the occupied reactive orbital also indicates that the electron distributions are localized to the enolate, as consistent with the direction of the electronic theory diagrams. This is also consistent with the result of the population analysis that the charge of the enolate is -0.887 (Mulliken) or -0.683 (Löwdin) after the dissociation. For this process, there is another unoccupied orbital giving almost the same orbital energy variation with the difference of only 0.06 kcal/mol (see Fig. S2 in the supporting information). Since this LUMO+3 has the electron distribution around the lone pair of O atom of the carbonyl group and the bonding π orbital of the C-C bond, the direction of charge transfer from the reactive orbitals becomes consistent with that of the electronic theory diagram. This result, therefore, may come from the misassignment due to the limit of the accuracy of the orbital energies. Furthermore, the occupied reactive orbital images show that the bond dissociation is attributed to the phase repulsion coming from the rotation of the dissociated C-O bond. The charge transferability index also shows the dynamics-driven nature of reaction (1). On the other hand, the reactive orbitals of reaction (2) indicate that the initial charge transfer direction in the backward process is consistent with that of the electronic theory diagram. The large charge transferability indices that this reaction initially proceeds through charge transfers. Since this contrasting result comes from the presence of the methyl group, this reveals how the methyl group, which do not participate in the reaction processes in the electronic theory diagrams, significantly affects the charge transferability index in reactions.

D. ROET analyses of isogyric reactions

Isogyric reactions are the reactions conserving the number of electron pairs. In the isogyric reactions, this study explores three bond formation reactions of methane (CH_4) molecule with formaldehyde, methanimine and nitrosyl hydride. Figure S1-6 in the supporting information draws the IRCs of these reactions with the reactant, product and TS geometries. In Fig. 8, the reactive orbitals and charge transferability indices of these isogyric reactions in the enolate-mode are shown.

For the forward processes, the figure shows that these reactions provide occupied reactive orbitals with analogous orbital shapes despite the corresponding molecule of reaction (3) being different from those of reactions (1) and (2): the π orbital of CH_3 anion for reactions (1) and (2) and the π orbital of OH anion for reaction (3). The unoccupied reactive orbitals are the π orbitals of formaldehyde and methanimine for reactions (1) and (2), respectively, while being the σ orbital of methane for reaction (3). For these reactions, the directions of charge transfers derived from the reactive orbitals are consistent with these electronic theory diagrams. The large charge transferability indices indicate that reaction (3) is CT-driven, while other reactions are dynamics-driven but close to CT-driven. From the variation of the occupied reactive orbitals, it is found that the charge transfers proceed through the antibonding π orbitals, which are induced by the approaches of the reactant molecules. This is an uninterpretable result in the electronic theory of organic chemistry, because no π orbitals appear in the sp^3 electronic state of methane.

The figure also indicates that the occupied reactive orbitals are the antibonding π orbitals of the double bonds of heteroatom anions, i.e., methanolate, methylamide and nitrosyl dihydride anions, while the unoccupied reactive orbitals being the antibonding π orbitals of ethane and methanol. For these backward processes, the directions of charge transfers are consistent with these electronic theory diagrams. The reactive indices determine that these processes are CT-driven. Similar to the forward processes, the variation of the occupied reactive orbitals show that these backward processes also proceed through the induced antibonding π orbitals. It is, therefore, concluded that the backward processes of these isogyric reactions are driven by charge transfers using antibonding π orbitals.

E. Exploration of the electronic theory of organic chemistry

Finally, let us check the ROET analysis results from the viewpoint of the electronic theory diagrams. The ROET analysis results fundamentally provide the same directions of charge transfer, which are determined by the occupied and unoccupied reactive orbitals of the reactant complexes, as those of the electronic theory diagrams for all reaction processes but the forward process of aldol reaction (2) in the enolate-mode and the backward process of α-aminooxylation reaction (1) in the forward and backward processes of 19 reactions (38 processes in total). Note that these results are consistent even for the functional groups of the charge transfer destinations. This suggests that the ROET serves a theoretical foundation for the electronic theory of organic chemistry, which has been empirically developed.

The ROET analyses also succeed to give theoretically-founded interpretations for organic bond formation reactions in acidic and basic conditions. In acidic conditions, organic bond formation reactions are usually performed by initially synthesizing carbocation intermediates and then forming reactive species like enols, which nucleophilically react through the conjugates with various orbitals. The ROET analyses of the enol-mode reactions reveal that the out-of-plane antibonding π orbitals centering on carbonyl carbons are conjugated with the antibonding orbitals of another molecule to form bonding orbitals, as is consistent with the bond formation mechanism of enols in the electronic theory of organic chemistry. On the other hand, carbanions are formed by deprotonating α-hydrogens in basic conditions, and then transform into reactive enolate anions, which are usually used to form bonds with α-carbons nucleophilically or with carbonyl carbons electrophilically. The ROET analyses of the enolate-mode reactions show that the in-plane antibonding π orbitals in the form of four-leaf clover centering on carbonyl carbons form bonds by sticking the leafstalk parts at α-carbons to carbonyl carbons and so on, as is also consistent with the bond formation mechanism of enolates in the electronic theory of organic chemistry. Therefore, the ROET analysis reproduces the bond formation reaction mechanisms in the electronic theory diagrams for both acidic and basic conditions, and theoretically explains the details of these bond formations such as the cause for the bond formations at α-carbons.

Furthermore, the ROET analyses have also revealed the detailed substituent effect of the methyl group. That is, the methyl group initially accepts electrons and then becomes electron resources to form new bonds. This result is reflected to the charge transferability

indices: in enol- and enolate-mode aldol reactions, the forward processes of reactions (2) and (4) provide higher charge transferability indices (i.e., CT-driven) than those of reactions (1) and (3), while the electron-accepting molecules contain the methyl groups in the formers, except for the forward process of reaction (4) in the enol-mode. This indicates that the ROET analysis can contribute to the prediction of the substituent effects in organic syntheses.

IV. CONCLUSIONS

In this study, we have compared the reactive orbital energy theory (ROET) to the uniquely-determined diagrams of the electronic theory of organic chemistry (the electronic theory diagrams) for the C-C and C-heteroatom bond formation reactions, i.e., aldol, Mannich, α-aminooxylation and isogyric reactions, The ROET is a reaction electronic theory for discussing reactions based on orbital energy variations [9, 10], which is developed independently of the electronic theory of organic chemistry. As a result, it is found that the ROET analyses fundamentally give the same charge transfer directions as those of the arrows in the electronic theory diagrams for all 38 reaction processes but only the forward process of aldol reaction (2) in the enolate-mode and the backward process of α-aminooxylation reaction (1). The ROET analyses reproduce even the functional groups of charge transfer destinations for these reaction processes. The remarkable correspondence of the ROET analyses and the electronic theory diagrams indicates that the ROET theoretically supports the rule-based electronic theory diagrams of organic chemistry.

The ROET analyses also reveal the organic bond formation mechanisms in acidic and basic conditions. Based on the ROET analyses, the enol-mode reactions in acidic conditions proceed using the out-of-plane antibonding π orbitals, while the enolate-mode reactions in basic conditions progress using the in-plane antibonding π orbitals in the form of four-leaf clover, both of which center on the carbonyl carbons. These findings explain the experimentally-assumed mechanisms of these bond formation reactions: e.g, the π-bond formations in acidic conditions and σ-bond formations at α-carbons in basic conditions. In addition, the ROET analyses show the detailed substituent effect of the methyl group: i.e., the methyl group initially accepts electrons and then donates them to the bond formations. These results suggest that the ROET analyses can theoretically reveal the electronic driving

forces of reactions as supported by the electronic theory of organic chemistry that has been experimentally demonstrated. Therefore, we confirm that the ROET serves a theoretical foundation for the electronic theory of organic chemistry.

Finally, the practical features of the ROET analysis, which will contribute to experimental analyses, are compiled as follows:

1. Different from the arrows in the electronic theory diagram of organic chemistry, the reactive orbitals of the ROET analysis are available as a theoretical evidence for synthetic reactions, because the ROET analysis contains no empirical processes for reproducing the electronic theory diagrams. The electronic motions, which are derived from the reactive orbitals, strongly support the predicted reaction pathways, if the electronic motions are consistent with those of the electronic theory diagrams.

2. The ROET analysis is also useful for designing efficient synthetic reactions, because it incorporates all the electronic effects to illustrate the electronic motions driving the reactions. For example, the substituent effects can be tested by checking the enhancement of the electronic motions of the reactive orbitals, as shown for the substituent effect of the methyl group in this study. Note that it is usually difficult to correctly predict the substituent effects using only the presumed resonance structures based on the electron-donating and -accepting abilities of the functional groups.

3. Furthermore, the ROET analysis is available as an easy check for predicting the reaction mechanisms, because it gives physically-meaningless electronic motions for the incorrect or multi-step reactions even though the reaction pathway provides reasonable resonance structures.

These features will be enhanced by developing a method for avoiding transition state geometry calculations in the ROET analysis in near future.

Acknowledgments

This research was financially supported by JST CREST, Japan (Grant No. JPMJCR1902).

Supporting Information Available

The IRCs, which are calculated in GRRM17 and Gaussian 16 programs, with the reactant, product and TS geometries for aldol reactions in the enol-mode (S1-1) and enolate-mode (S1-2), Mannich reactions in the enol-mode (S1-3) and enolate-mode (S1-4), α-aminooxylation reactions (S1-5) and isogyric reactions (S1-6) are compiled in Figs. S1 of the supporting information file. The orbital energy variations on the normalized IRCs are also given in Fig. S2. The alternative ROET analysis result for the backward process of α-aminooxylation reaction (1) in enolate-mode is also illustrated in Fig. S3. In Fig. S4, the Cartesian coordinates of the geometries of the reactant complexes, transition states, and product complexes of all these reactions are compiled.

Data Availability statement

The data generated and/or analyzed in this study are available from the correponding author, Takao Tsuneda, upon reasonable request.

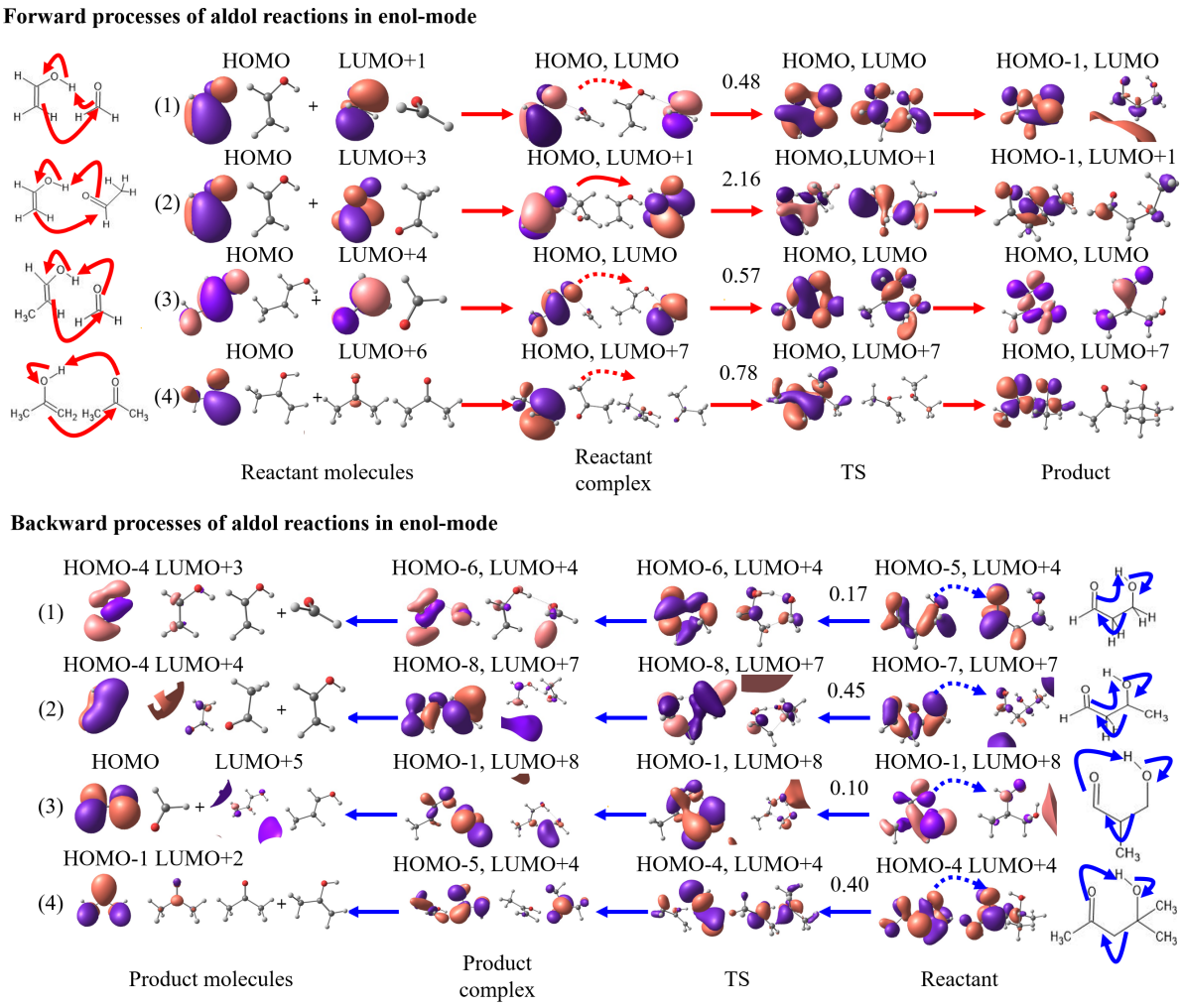

FIG. 3: The occupied and unoccupied reactive orbital pairs of four aldol reactions in the enol-mode for the forward bond formation and backward bond dissociation processes. For the reactant and product molecules, the reactive orbitals corresponding to those of the reactant and product complexes are shown with the orbital level names for these molecules. The numbers in between the reactive orbitals of the reactant complexes and those of the transition state (TS) structures indicate the charge transferability indices of the reactive orbital energy theory. In the reactive orbitals of the reactant complexes, dotted arrows are illustrated to show that these reactions are determined as "dynamics-driven". The electronic theory diagrams are also attached at the leftmost and rightmost for the forward and backward processes, respectively.

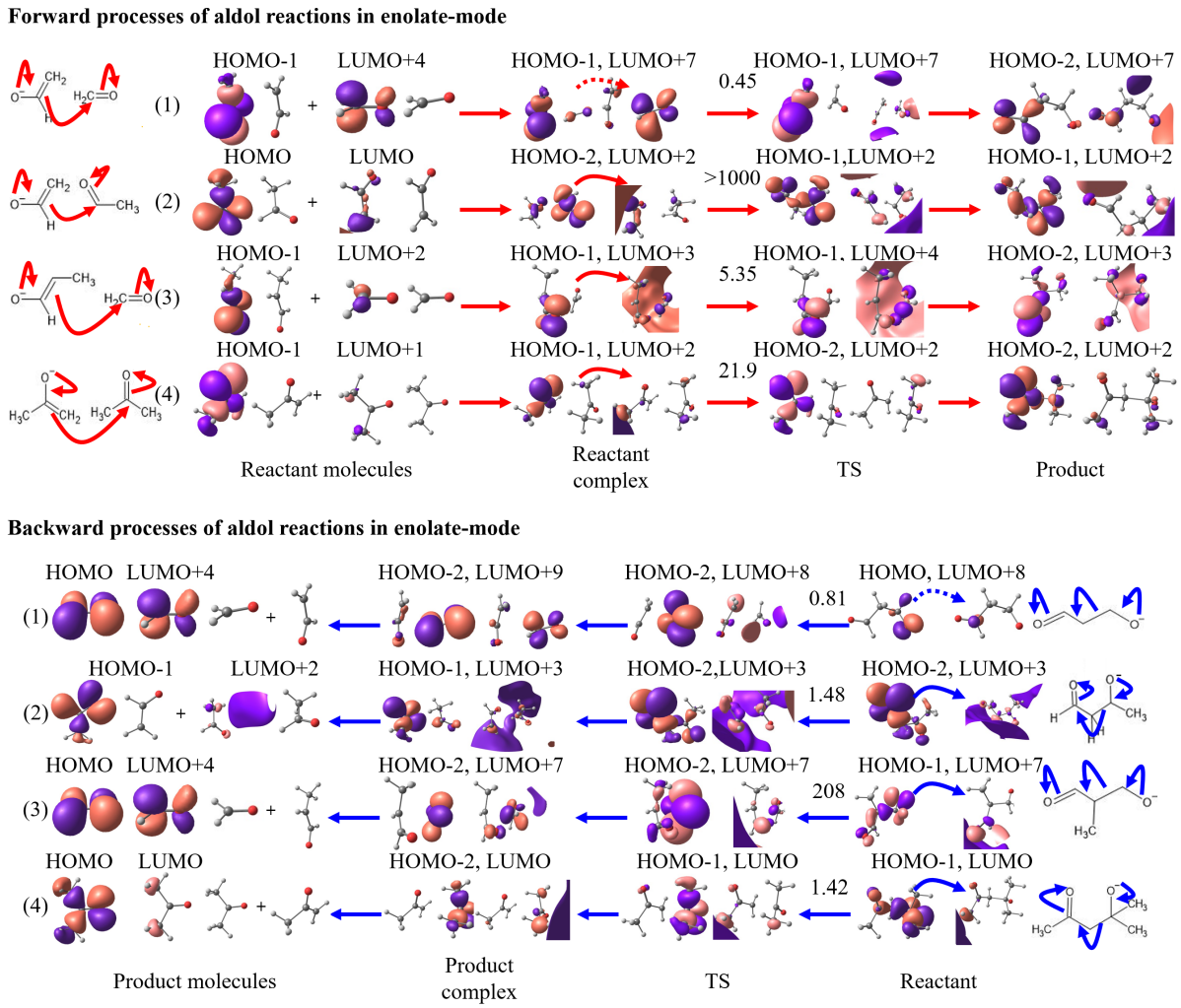

FIG. 4: The occupied and unoccupied reactive orbital pairs of four aldol reactions in the enolate-mode for the forward and backward processes. For the reactant and product molecules, the reactive orbitals corresponding to those of the reactant and product complexes are shown with the orbital level names for these molecules. The numbers in between the reactive orbitals of the reactant complexes and those of the transition state (TS) structures indicate the charge transferability indices of the reactive orbital energy theory. In the reactive orbitals of the reactant complexes, dotted arrows are illustrated to show that these reactions are determined as "dynamics-driven", while solid arrows are drawn to indicate that these reactions are "charge transfer-driven". The electronic theory diagrams are also attached at the leftmost and rightmost for the forward and backward processes, respectively.

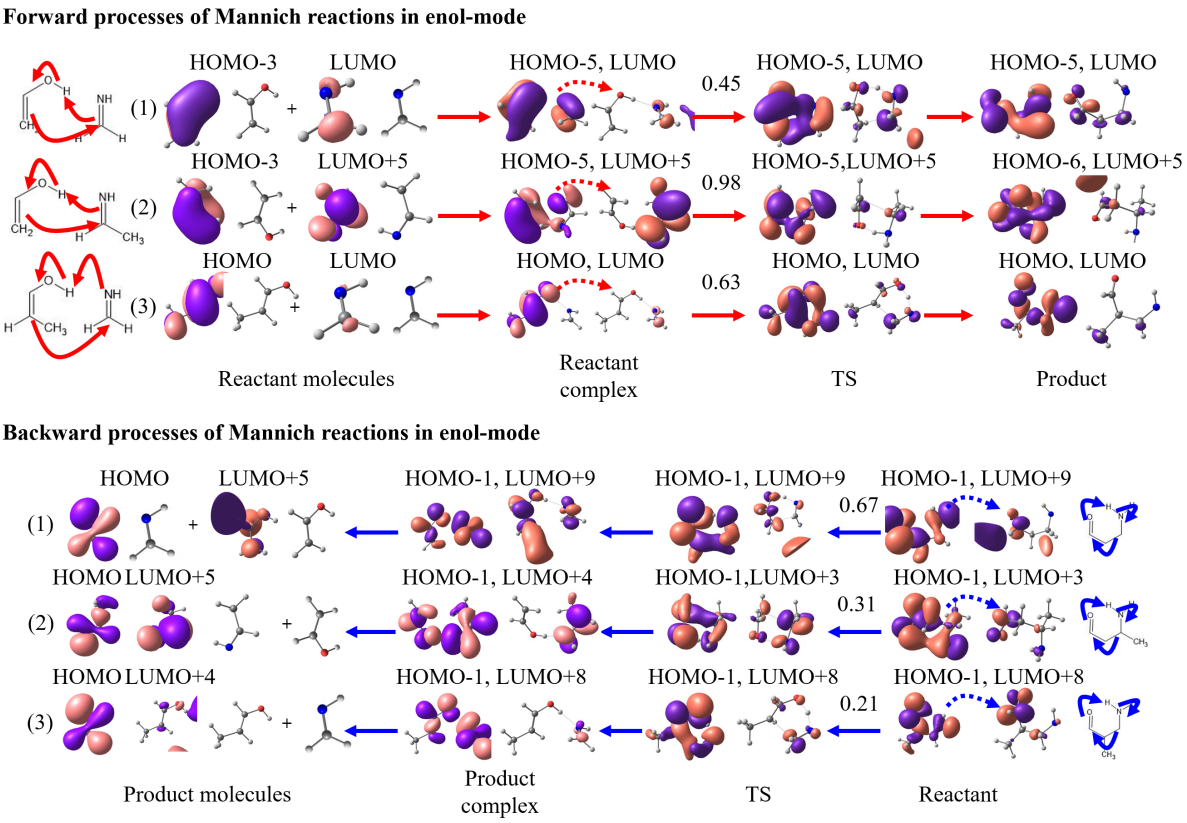

FIG. 5: The occupied and unoccupied reactive orbital pairs of three Mannich reactions in the enol-mode for the forward bond formation and backward bond dissociation processes. For the reactant and product molecules, the reactive orbitals corresponding to those of the reactant and product complexes are shown with the orbital level names for these molecules. The numbers in between the reactive orbitals of the reactant complexes and those of the transition state (TS) structures indicate the charge transferability indices of the reactive orbital energy theory. In the reactive orbitals of the reactant complexes, dotted arrows are illustrated to show that these reactions are determined as "dynamics-driven", while solid arrows are drawn to indicate that these reactions are "charge transfer-driven". The electronic theory diagrams are also attached at the leftmost and rightmost for the forward and backward processes, respectively.

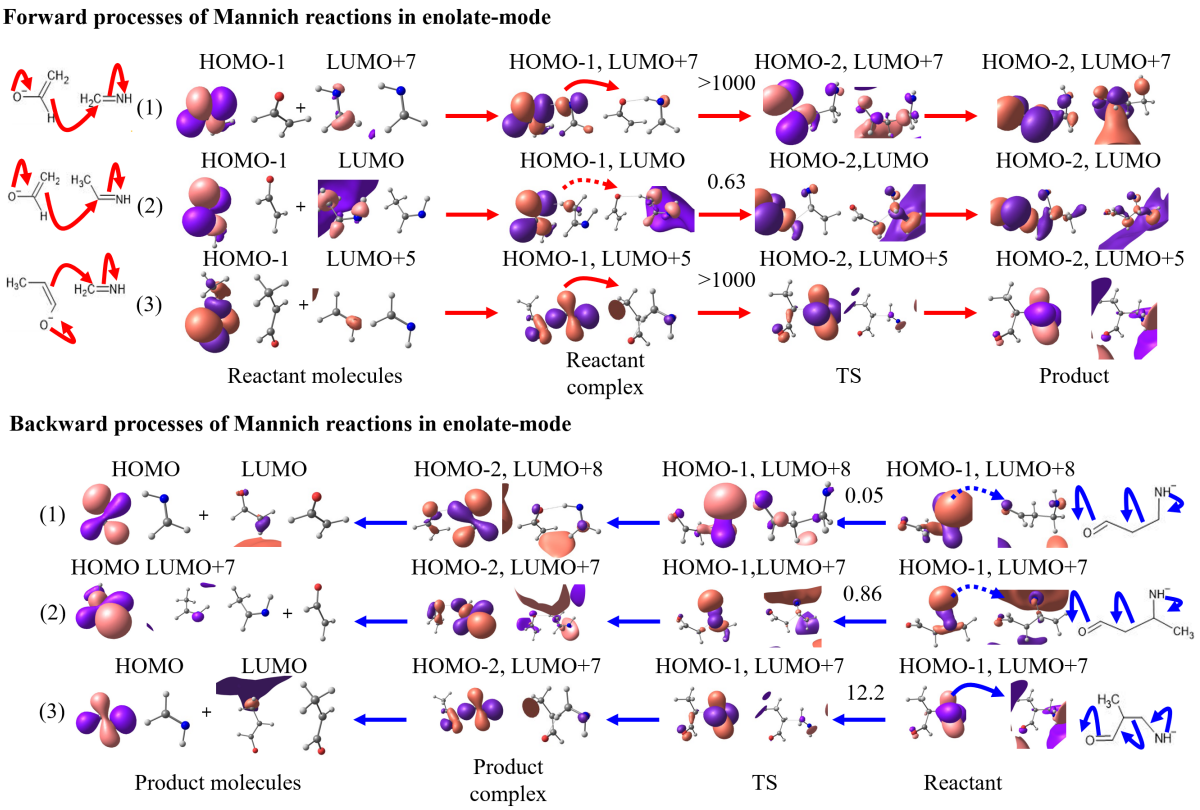

FIG. 6: The occupied and unoccupied reactive orbital pairs of three Mannich reactions in the enolate-mode for the forward bond formation and backward bond dissociation processes. For the reactant and product molecules, the reactive orbitals corresponding to those of the reactant and product complexes are shown with the orbital level names for these molecules. The numbers in between the reactive orbitals of the reactant complexes and those of the transition state (TS) structures indicate the charge transferability indices of the reactive orbital energy theory. In the reactive orbitals of the reactant complexes, dotted arrows are illustrated to show that these reactions are determined as "dynamics-driven", while solid arrows are drawn to indicate that these reactions are "charge transfer-driven". The electronic theory diagrams are also attached at the leftmost and rightmost for the forward and backward processes, respectively.

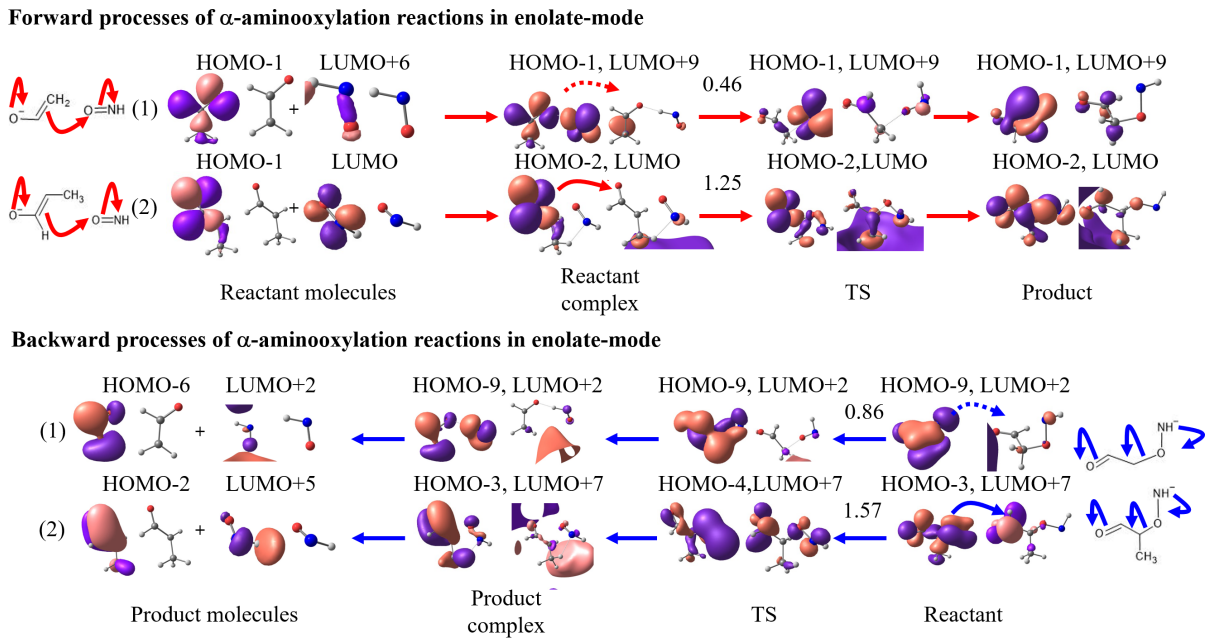

FIG. 7: The occupied and unoccupied reactive orbital pairs of two α-aminooxylation reactions in the enolate-mode for the forward bond formation and backward bond dissociation processes. For the reactant and product molecules, the reactive orbitals corresponding to those of the reactant and product complexes are shown with the orbital level names for these molecules. The numbers in between the reactive orbitals of the reactant complexes and those of the transition state (TS) structures indicate the charge transferability indices of the reactive orbital energy theory. In the reactive orbitals of the reactant complexes, dotted arrows are illustrated to show that these reactions are determined as "dynamics-driven", while solid arrows are drawn to indicate that these reactions are "charge transfer-driven". The electronic theory diagrams are also attached at the leftmost and rightmost for the forward and backward processes, respectively.

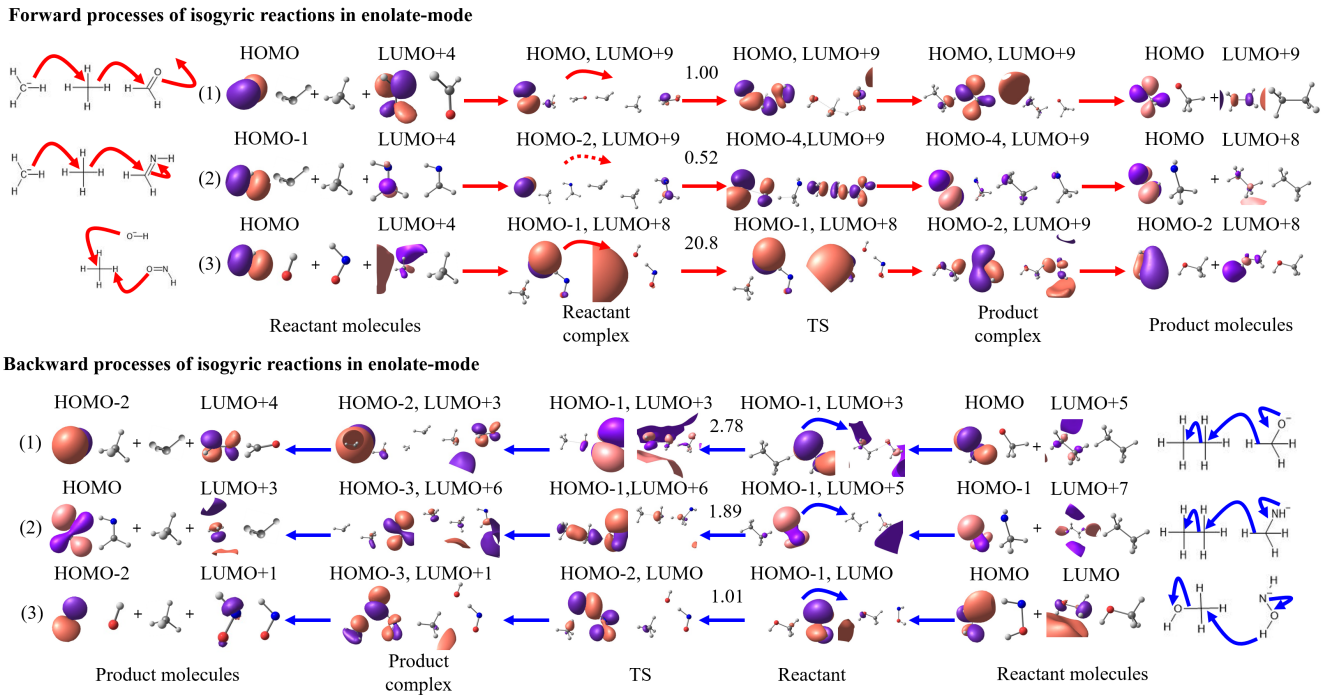

FIG. 8: The occupied and unoccupied reactive orbital pairs of three isogyric reactions in the enolate-mode for the forward bond formation and backward bond dissociation processes. For the reactant and product molecules, the reactive orbitals corresponding to those of the reactant and product complexes are shown with the orbital level names for these molecules. The numbers in between the reactive orbitals of the reactant complexes and those of the transition state (TS) structures indicate the charge transferability indices of the reactive orbital energy theory. In the reactive orbitals of the reactant complexes, dotted arrows are illustrated to show that these reactions are determined as "dynamics-driven", while solid arrows are drawn to indicate that these reactions are "charge transfer-driven". The electronic theory diagrams are also attached at the leftmost and rightmost for the forward and backward processes, respectively.

Figure Captions

Fig. 1. Calculated reactions: four aldol, three Mannich, two α-aminooxylation and three isogyric reactions.

Fig. 2. Enol- and enolate-mode mechanisms of calculated ketones for aldol and Mannich reactions.

Fig. 3. The occupied and unoccupied reactive orbital pairs of four aldol reactions in the enol-mode for the forward bond formation and backward bond dissociation processes. For the reactant and product molecules, the reactive orbitals corresponding to those of the reactant and product complexes are shown with the orbital level names for these molecules. The numbers in between the reactive orbitals of the reactant complexes and those of the transition state (TS) structures indicate the charge transferability indices of the reactive orbital energy theory. In the reactive orbitals of the reactant complexes, dotted arrows are illustrated to show that these reactions are determined as "dynamics-driven". The electronic theory diagrams are also attached at the leftmost and rightmost for the forward and backward processes, respectively.

Fig. 4. The occupied and unoccupied reactive orbital pairs of four aldol reactions in the enolate-mode for the forward and backward processes. For the reactant and product molecules, the reactive orbitals corresponding to those of the reactant and product complexes are shown with the orbital level names for these molecules. The numbers in between the reactive orbitals of the reactant complexes and those of the transition state (TS) structures indicate the charge transferability indices of the reactive orbital energy theory. In the reactive orbitals of the reactant complexes, dotted arrows are illustrated to show that these reactions are determined as "dynamics-driven", while solid arrows are drawn to indicate that these reactions are "charge transfer-driven". The electronic theory diagrams are also attached at the leftmost and rightmost for the forward and backward processes, respectively.

Fig. 5. The occupied and unoccupied reactive orbital pairs of three Mannich reactions in the enol-mode for the forward bond formation and backward bond dissociation processes.

For the reactant and product molecules, the reactive orbitals corresponding to those of the reactant and product complexes are shown with the orbital level names for these molecules. The numbers in between the reactive orbitals of the reactant complexes and those of the transition state (TS) structures indicate the charge transferability indices of the reactive orbital energy theory. In the reactive orbitals of the reactant complexes, dotted arrows are illustrated to show that these reactions are determined as "dynamics-driven", while solid arrows are drawn to indicate that these reactions are "charge transfer-driven". The electronic theory diagrams are also attached at the leftmost and rightmost for the forward and backward processes, respectively.

Fig. 6. The occupied and unoccupied reactive orbital pairs of four aldol reactions in the enolate-mode for the forward and backward processes. For the reactant and product molecules, the reactive orbitals corresponding to those of the reactant and product complexes are shown with the orbital level names for these molecules. The numbers in between the reactive orbitals of the reactant complexes and those of the transition state (TS) structures indicate the charge transferability indices of the reactive orbital energy theory. In the reactive orbitals of the reactant complexes, dotted arrows are illustrated to show that these reactions are determined as "dynamics-driven", while solid arrows are drawn to indicate that these reactions are "charge transfer-driven". The electronic theory diagrams are also attached at the leftmost and rightmost for the forward and backward processes, respectively.

Fig. 7. The occupied and unoccupied reactive orbital pairs of two α-aminooxylation reactions in the enolate-mode for the forward bond formation and backward bond dissociation processes. For the reactant and product molecules, the reactive orbitals corresponding to those of the reactant and product complexes are shown with the orbital level names for these molecules. The numbers in between the reactive orbitals of the reactant complexes and those of the transition state (TS) structures indicate the charge transferability indices of the reactive orbital energy theory. In the reactive orbitals of the reactant complexes, dotted arrows are illustrated to show that these reactions are determined as "dynamics-driven", while solid arrows are drawn to indicate that these reactions are "charge transfer-driven". The electronic theory diagrams are also attached at the leftmost and rightmost for the

forward and backward processes, respectively.

Fig. 8. The occupied and unoccupied reactive orbital pairs of three isogyric reactions in the enolate-mode for the forward bond formation and backward bond dissociation processes. For the reactant and product molecules, the reactive orbitals corresponding to those of the reactant and product complexes are shown with the orbital level names for these molecules. The numbers in between the reactive orbitals of the reactant complexes and those of the transition state (TS) structures indicate the charge transferability indices of the reactive orbital energy theory. In the reactive orbitals of the reactant complexes, dotted arrows are illustrated to show that these reactions are determined as "dynamics-driven", while solid arrows are drawn to indicate that these reactions are "charge transfer-driven". The electronic theory diagrams are also attached at the leftmost and rightmost for the forward and backward processes, respectively.

[1] G. N. Lewis, J. Am. Chem. Soc. **38**, 762 (1916).

[2] C. K. Ingold, Chem. Rev. **15**, 225 (1934).

[3] K. Fukui, T. Yonezawa, and H. Shingu, J. Chem. Phys. **20**, 722 (1952).

[4] P. A. Johnson, L. J. Bartolotti, P. W. Ayers, T. Fievez, and P. Geerlings, in *Modern Charge Density Analysis*, edited by C. Gatti and P. Macchi (Springer, New York, 2012), pp. 715–764.

[5] F. De Proft, P. Geerlings, and P. W. Ayers, in *The chemical bond: Fundamental aspects of chemical bonding*, edited by S. Shaik and G. Frenking (Wiley, Darmstadt, 2014), vol. 1, pp. 233–270.

[6] P. Geerlings, E. Chamorro, P. K. Chattaraj, F. D. Proft, J. L. Gazquez, S. Liu, C. Morell, A. Toro-Labbe, A. Vela, and P. Ayers, Theor. Chem. Acc. **139**, 36(1 (2020).

[7] R. B. Grossman, *The Art of Writing Reasonable Organic Reaction Mechanisms, 2nd Ed.* (Springer, New York, 2003).

[8] R. F. Nalewajski and R. G. Parr, J. Chem. Phys. **77**, 399 (1982).

[9] T. Tsuneda and R. K. Singh, J. Comput. Chem. **35**, 1093 (2014).

[10] T. Tsuneda, R. K. Singh, and P. K. Chattaraj, Phys. Chem. Chem. Phys. **20**, 14211 (2018).

[11] T. Tsuneda, S. Maeda, Y. Harabuchi, and R. K. Singh, Computation **4**, 23 (2016).

[12] J. P. Perdew, R. G. Parr, M. Levy, and J. L. J. Balduz, Phys. Rev. Lett. **49**, 1691 (1982).

[13] T. Tsuneda, J.-W. Song, S. Suzuki, and K. Hirao, J. Chem. Phys. **133**, 174101(1 (2010).

[14] R. K. Singh and T. Tsuneda, J. Comput. Chem. **34**, 379 (2013).

[15] M. Hasebe, T. Tsutsumi, T. Taketsugu, and T. Tsuneda, J. Chem. Theory Comput. **17**, 6901 (2021).

[16] A. Cordova, H. Sunden, A. Bogevig, M. Johansson, and F. Himo, Chem. Eur. J. **10**, 3673 (2004).

[17] B. List, Tetrahedron **58**, 5573 (2002).

[18] R. K. Singh, T. Tsuneda, and K. Hirao, Theor. Chem. Acc. **130**, 153 (2011).

[19] W. Kohn and L. J. Sham, Phys. Rev. A **140**, 1133 (1965).

[20] T. Tsuneda, *Density Functional Theory in Quantum Chemistry* (Springer, Tokyo, 2014).

[21] M. Kamiya, T. Tsuneda, and K. Hirao, J. Chem. Phys. **117**, 6010 (2002).

[22] T. Tsuneda and T. Taketsugu, in *π-Stacked Polymers and Molecules: Theory, Synthesis, and*

Properties, edited by T. Nakano (Springer, Tokyo, 2013).

[23] H. Iikura, T. Tsuneda, T. Yanai, and K. Hirao, J. Chem. Phys. **115**, 3540 (2001).

[24] Y. Tawada, T. Tsuneda, S. Yanagisawa, T. Yanai, and K. Hirao, J. Chem. Phys. **120**, 8425 (2004).

[25] T. Tsuneda and K. Hirao, WIREs Comput. Mol. Sci. **4**, 375 (2014).

[26] T. Sato and H. Nakai, J. Chem. Phys. **131**, 224104 (2009).

[27] A. D. Becke, Phys. Rev. A **38**, 3098 (1988).

[28] T. Tsuneda, T. Suzumura, and K. Hirao, J. Chem. Phys. **110**, 10664 (1999).

[29] R. A. Kendall, T. H. Dunning Jr., and R. J. Harrison, J. Chem. Phys. **96**, 6796 (1992).

[30] S. Maeda, Y. Harabuchi, M. Takagi, K. Saita, K. Suzuki, T. Ichino, Y. Sumiya, K. Sugiyama, and Y. Ono, J. Comput. Chem. **39**, 233 (2018).

[31] S. Maeda, Y. Harabuchi, Y. Sumiya, M. Takagi, K. Suzuki, M. Hatanaka, Y. Osada, T. Taketsugu, K. Morokuma, and K. Ohno, *Grrm17* (2017), http://iqce.jp/GRRM/index_e.shtml.

[32] S. Maeda, K. Ohno, and K. Morokuma, Phys. Chem. Chem. Phys. **15**, 3683 (2013).

[33] C. Gonzalez and H. B. Schlegel, J. Chem. Phys. **90**, 2154 (1989).

[34] M. W. Schmidt, K. K. Baldridge, J. A. Boatz, S. T. Elbert, M. S. Gordon, J. H. Jensen, S. Koseki, N. Matsunaga, K. A. Nguyen, S. Su, et al., J. Comput. Chem. **14**, 1347 (1993).